Dropwise Condensation Water Drainage Model

Marcus Richardson[1] Robert Kunz[2]

[1]The Boeing Company, USA, {marcus.k.richardson}@boeing.com
[2]Mechanical Engineering, Pennsylvania State University, USA, {rkf102}@psu.edu

Abstract

Modeling of condensation is important to predicting the amount of residual water in small channels. The residual water that forms becomes a source of humidity for permeable materials such as wooden structure and insulation. A Modelica model has been implemented that predicts the amount of residual moisture after a period of water build up. The model has a very low computational requirement and runs in minutes on a desktop computer. This model includes parameters to relate droplet physics to a control volume. The parameters provide a macroscopic means of varying droplet adhesion force, droplet velocity, and drainage dynamics. Using CFD data as an example of real world data, this model has been correlated to demonstrate the effects of the parameters. This model enables analytical prediction of the amount of time that is needed to dry the internal surfaces of an aircraft after flight and may be connected to a diffusion model for permeable materials.
Keywords: condensation, Droplet Distribution

1 Introduction

Research into mathematical condensation modeling was motivated by the author's experience with aircraft moisture management. Aircraft operators have struggled with managing the effects of condensate since the mid-20th century (Huber, Schuster, and Townsend 1999). Uncontrolled condensation leads to uncomfortable passenger experiences, costly maintenance actions, and extra weight, where every pound counts. Accumulated water in passenger aircraft contributes to moisture related problems, including structure corrosion, uncontrolled water flow, increased fuel consumption, higher maintenance costs and mold growth (Wörner et al. 2002). The insulation systems are heavily impacted by condensation. An aircraft insulation system comprises fiberglass batting and cover films that enclose the insulation. The insulation system is installed around the circumference of the fuselage and extends from the flight deck to the back of the airplane (see figures 1 and 2). To improve and test their designs, aircraft manufacturers invest substantially in designs and test methods (Connell and Richardson 2022; Connell, Carnegie, and Richardson 2020; Richardson, Imada, and Sarinas 2021; Khashayer et al. 2019). When summed for the whole airplane, moisture absorption into the blankets can result in a measurable weight increase. Each pound of moisture can translate to 0.03 pounds or more of extra fuel consumption per flight (Lents 2021).

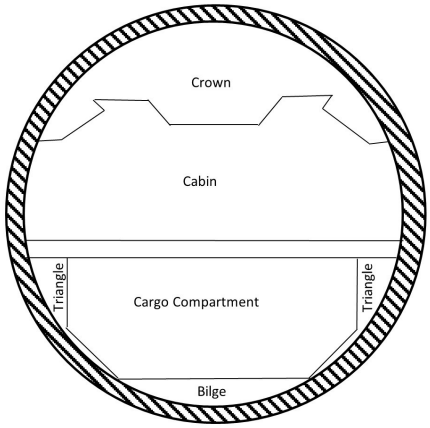

Figure 1. Insulation is typically installed around the circumference of an aircraft monocoque adapted from (Connell and Richardson 2022).

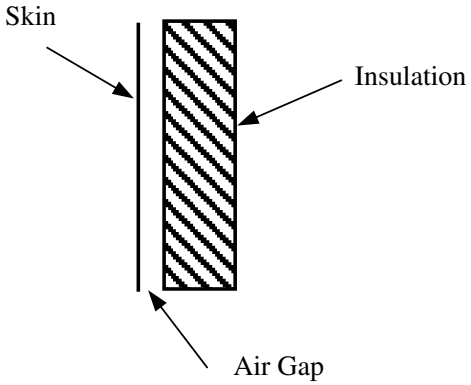

Figure 2. A typical insulation blanket leaves a gap between the skin and the insulation (Wörner et al. 2002).

Droplet motion is a critical aspect of condensation. Droplet motion, particularly dropwise condensation, has been studied since the 1930s because it was reported to have a much higher heat transfer coefficient than film condensation. Although, mass transfer was not the motivation of the studies, the dominant mode of heat transfer was the latent heat of condensation and evaporation (mass

and heat transfer). The mass transfer rate is affected by the density of droplets and type of condensation. Droplet density is defined here as the number of droplets per unit surface area. Rose et al. provide a seminal work on the distribution of droplets on a surface (Rose and Glicksman 1973; Rose 1976), also referred to as the Rose droplet distribution curve. It was extended to low pressure ambient environments (saturation temperature of 31°C) and reproduced later (Graham and Griffith 1973). These researchers studied dropwise condensation on a vertical surface, observing droplets forming, coalescing and falling such that under steady-state conditions a maximum droplet size was noted. Rose and Glicksman broke up the process into generations of droplets. Their examination of the data revealed two key parameters, the fraction of available area and the ratio of the maximum radius of a current generation of droplets to its predecessors. The paper develops a calculation method and presents a comparison with the test data (Rose and Glicksman 1973).

Water droplets on inclined surfaces have an internal flow field that affects the rate at which the droplet moves. The droplet internal flow field, adhesion forces, and surface inclination angle on a hydrophilic surface have been related by CFD simulations and experimental tests (Al-Sharafi et al. 2020). This study determined that the shear force term in the force balance for a water droplet is negligible. The paper provides droplet geometry models and a table of advancing and receding contact angles, each for a variety of droplet volumes and surface inclination angles.

Condensation and management of the residual water is an important topic to the aircraft industry (Wörner et al. 2002; Huber, Schuster, and Townsend 1999; Liu, Aizawa, and Yoshino 2004). The current focus of the aerospace industry on digital twins (Meyer et al. 2020; Arthur et al. 2020), and modern cyber-physical engineering design trends (Sztipanovits et al. 2012; Seshia et al. 2017) present a need for models of varying fidelity with varying computational performance demands.

The topic of condensation includes both the interfacial mass transfer (Gu, Min, and Tang 2018; Steeman et al. 2009) and the motion models for the condensate. The dropwise condensation models typically focus on a constant generation source to enable steady-state estimations of heat transfer rates on various surfaces (Weisensee et al. 2017; Grooten and Van Der Geld 2012). However, there is a gap when it comes to determining the residual moisture, or the droplets that are left after the temperature of the surface has risen above the dew point. Furthermore, many papers provide a good description of modeling methods (Rose and Glicksman 1973; Graham and Griffith 1973) but none have applied them to a Modelica model, and few have integrated the droplet physics models (Al-Sharafi et al. 2020; Pilat et al. 2012; Sun et al. 2020). This paper proposes a hybrid model that uses a detailed droplet force balance model in conjunction with the Rose distribution curve to determine the residual moisture on a surface. This Modelica model complements the existing work (Casella et al. 2006; Norrefeldt, Grün, and Sedlbauer 2012). The paper is organized as follows: section 2 describes the fundamental dropwise condensation equations, section 3 presents the Modelica implementation and its comparison with a Star CCM+ CFD model, section 4 reports the results of an implementation of the Modelica model that exercises all the functions the model, and section 5 is the conclusion.

2 Dropwise Condensation Equations

The conservation equations (1, 2, 3) are applied to a control volume, which represents the total volume of water on the surface. However, A force balance on the largest droplet on the surface is added to the momentum equation, integrating the physics of the control volume with that of the largest droplet on the surface. This allows the model to initiate droplet motion when the largest droplet reaches a critical size. It also simulates the sweeping of other droplets in the path of the largest droplet by integrating the control volume and the droplet physics.

$$\frac{\partial \rho}{\partial t}\forall = \dot{m}_x + \dot{m}_{x+\Delta x} + \Gamma \tag{1}$$

$$\frac{\partial \rho v}{\partial t}\forall = (\dot{m}v)_x + (\dot{m}v)_{x+\Delta x} + \zeta(\eta F_{ad} + F_g) \tag{2}$$

$$\frac{\partial \rho h}{\partial t}\forall = (\dot{m}h)_x + (\dot{m}h)_{x+\Delta x} + Q_{plate} + Q_{latent} \tag{3}$$

Where $\dot{m}$ is the liquid mass flow rate, $\forall$ is the total water volume, $\Gamma$is the interfacial mass transfer rate. The subscripts *ad* and *g* of the force term are adhesion and gravity. The subscripts x and x+δx indicate the upper and lower edge of a control volume. ζ and η are parameters that have been added to calibrate the model. ρ is density, h is specific enthalpy, and Q is heat transfer. Q_{plate} is the conductive and convective heat transfer from the plate to the water assuming the thickness of the largest droplet and Q_{latent} applies the heat of vaporization and condensation to the control volume.

The velocity of the water droplets is determined by the velocity factor (v_f,4).

$$\dot{m}_{x+\Delta x} = m\frac{v}{v_f} \tag{4}$$

The condensation rate is calculated using equations 5, 6, 7, 8, and 9. A, c, p, D, α, cp, subscript *inf*, and subscript *s* represent area, water vapor concentration, pressure, the diffusion factor, thermal diffusivity, specific heat, fluid free stream properties, and surface. The heat transfer coefficient (h) was set to 10 $\frac{W}{m^2 \deg K}$ and the diffusion factor was set to 2.6 e-5 $\frac{m^2}{s}$.h_m is the mass transfer coefficient.

$$\Gamma = h_m \rho_{H2Ovapor} A_s (c_s - c_{inf}) \tag{5}$$

$$h_m = \frac{h}{\rho_{air} c_{p-air}} \left(\frac{D}{\alpha_{air}}\right)^{\frac{2}{3}} \tag{6}$$

$$c_s - c_{\inf} \approx \frac{p_{sat} - p_{H2O,\inf}}{p_{\inf}} \tag{7}$$

$$A_{dry} = A_s - A_{wet} \tag{8}$$

The hyberbolic tangent function is used to prevent the evaporation function from producing a negative mass on the surface.

$$A_s(\Gamma, mass) = \begin{cases} A_{dry}, & \text{if } \Gamma > 0 \\ A_{dry}\left(\frac{1+tanh(\beta(mass-mass_{min}))}{2}\right), & \text{else} \end{cases} \tag{9}$$

The droplet adhesion force F_{AD} is determined by equations 10 and 11 with advancing and receding contact angles (θ_A and θ_R) for a hydrophilic surface (Al-Sharafi et al. 2020). The variables d, γ_{SL}, γ_{LV} are the droplet diameter, solid-liquid surface tension, and liquid-vapor surface tension. θ_{ave} is the average of the advancing and receding contact angles.

$$F_{AD} \approx \frac{24}{\pi^3} \gamma_{SL} d (cos(\theta_R) - cos(\theta_A)) \tag{10}$$

$$cos(\theta_{ave}) = \frac{\gamma_{SL}}{\gamma_{LV}} \tag{11}$$

The droplet distribution curve (Graham and Griffith 1973) (13) is critical to predicting the diameter of the largest droplet on the surface as a function of total water volume and the water droplet volume model (12).

$$\forall = \frac{\pi}{24} \frac{d^3}{sin^3 \theta_{ave}} [2 + cos\theta_{ave}][1 - cos\theta_{ave}]^2 \tag{12}$$

$$N_o = 0.05 d^{-2} \tag{13}$$

$$\forall_{tot} = B[d_{max} - d_{min}] \tag{14}$$

$$B = \frac{A_s \pi}{160} \frac{[2 + cos\theta_{ave}][1 - cos\theta_{ave}]^2}{sin^3 \theta_{ave}} \tag{15}$$

$$d_{max} = \frac{\forall_{tot}}{B} + d_{min} \tag{16}$$

$$A_{wet} = \frac{A_s \pi}{40} [ln(d_{max}) - ln(d_{min})] \tag{17}$$

3 Modelica Implementation and Verification

The modelica implementation sought to take advantage of existing Modelica Library components. The standard water model, fluid library ports, and thermal libary components were used as shown in figure 4. This model calculates the conservation equations for the water on the surface and the surface temperature. The entire model is displayed in figure 3. The water state was treated as a hyberbolic tangent function (18) to prevent events. The temperature of the water was limited to above freezing to prevent range errors. Due to this limitation, the temperature of the surface was used to determine the solid/liquid state of the water. The Modelica tables contain the advancing and receding contact angles. The thermal mass represents the mass of the plate.

The surface model includes one thermal port for contact with the air in the channel, another for contact with an exterior heat transfer source, a real input to receive the average velocity of the water flowing into the surface, a real output to report the same velocity flowing out of the surface, three fluid ports to transfer water by interfacial mass transfer (portHorizontal) and allow water to flow from the upper surfaces to the lower surfaces. The Modelica Library prescribed heat flow component was used to transfer heat from the surface to the water droplets.

$$WS = \frac{1 + tanh(\alpha(T - 273.15) + 1)}{2} \tag{18}$$

The surface model was connected to a buoyant air volume (blue-green box in figure 3), which calculates the condensation rate and transfers it across a fluid port. The buoyant air volume applies a pressure correction to the upper and lower fluid ports, which acts as a motive force for moist air to be drawn into the volume in the upper port and ejected out the lower port when the air is being cooled. The heat transfer port applies the convection heat transfer of the channel air to the surface and the real input port receives the dry surface area of the plate.

The Star-CCM+ CFD model used a fluid film model that included as inputs the nucleation density (N) and the minimum diameter radius diameter. It distributes the mass of water on the surface into a constant number of droplets, as specified by the nucleation density. A film begins to flow when the calculated droplet radius exceeds the minimum allowed, which is set by the user. A translation was developed to equivocate the film thickness (H), being the fraction of the volume of water to the surface area, to droplet diameter using the same nucleation density as the CFD model (Equation 19). The surface was maintained at 274°K and the air was supplied at at 300°K, with a velocity of 1.0 $\frac{m}{s}$, a moist air mass fraction of 0.023 $\frac{H2O}{totalmass}$ and pressure of 101,326 Pa.

$$d = \left(\frac{12H}{\pi N}\right)^{\frac{1}{3}} \tag{19}$$

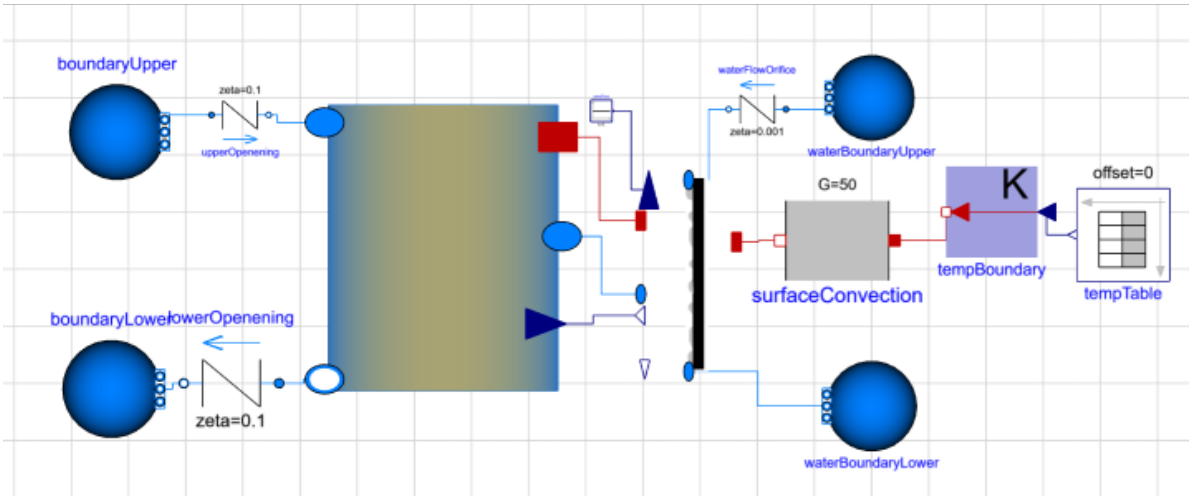

Figure 3. The 1-D model for comparison with the CFD model.

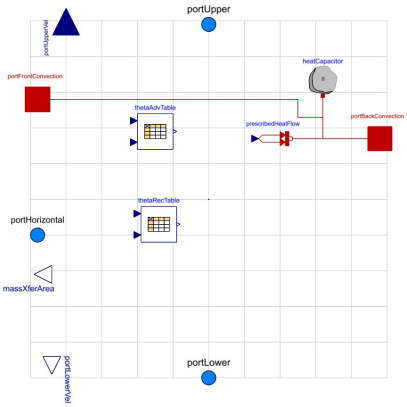

Figure 4. The surface model.

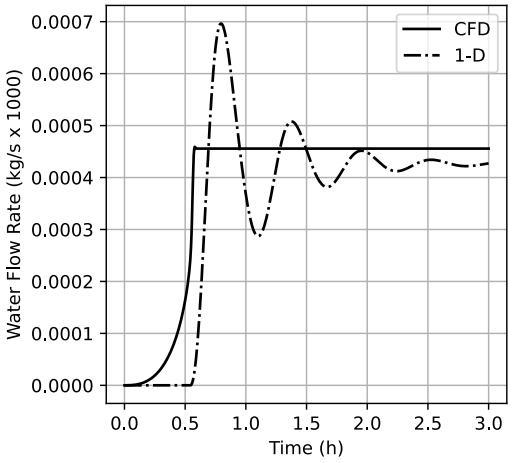

Figure 5. A comparison of the CFD and 1-D Modelica model water flow rates.

Figure 5 verifies that the drainage rates in the CFD and 1-D Modelica Model were close. Figure 6 verifies that the average film thickness was the same in both models.

The parameters ζ and v_f and η were varied to study their effect on the film thickness and water flow rate. ζ scales the value of the force balance on a single droplet. The velocity factor can be tuned to the average velocity of the droplets draining off the surface. The variable η was added to adjust the steady-state film thickness, the steady-state droplet diameter, and the departure point of the droplets (the moment when the water begins to drain). The results are shown in figures 7 to 10, with parameter values given in table 1.

The oscillatory behavior of figures 5 and 6 is caused by the momentum equation. ζ and v_f effect the frequency, amplitude, and decay rate of the water flow rate. v_f can be constrained to an experimentally observed average droplet velocity, leaving variation of ζ for final tuning of the model. It is dampened by decreasing ζ. The oscillatory behavior is a symptom of using a continuous conservation equation to describe a discontinuous process of droplets growing, sliding, and growing again. Once the velocity factor has been tuned ζ should be adjusted to ensure that the average film thickness response approximates the observed values.

Figures 7 and 8 present the effects of varying ζ. Increasing ζ minimizes the amount of initial water buildup on the surface and decreases the stabilization time. Figures 9 and 10 show that an increase in η increases the maximum steady-state volume of water that the surface will hold. η scales the adhesion force of the consevation equation (2).

4 Complete Model Simulation Results

The complete model simulates typical flight conditions by applying the temperature profile of figure 12 to a temper-

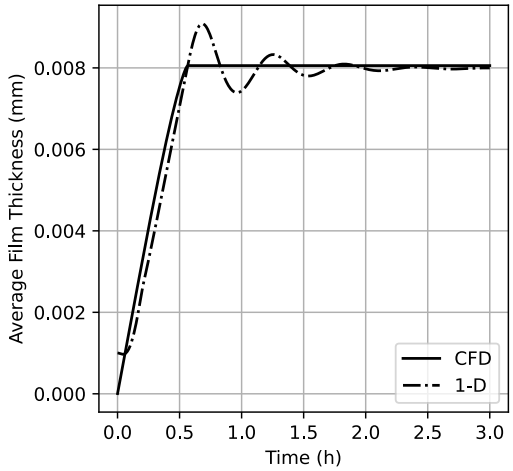

Figure 6. A comparison of the CFD and 1-D Modelica film thickness.

Table 1. Parameter Variations

Case Index	ζ	v_f (m)	η
1	0.5	1000	0.1
2	1.0	1000	0.1
3	1.5	1000	0.1
4	0.5	10	0.1
5	1.0	10	0.1
6	1.5	10	0.1
7*	1.0	10	1.0

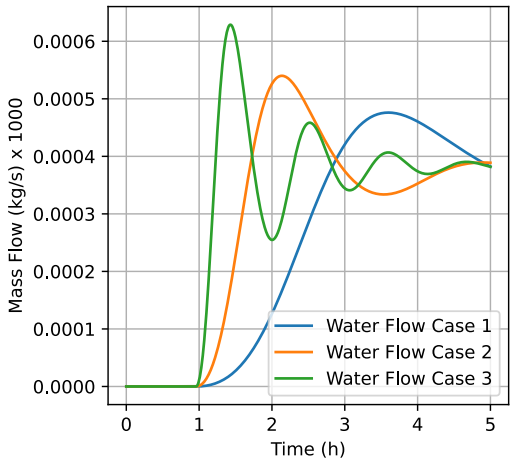

Figure 7. Parametric results water flow rate (cases 1 to 3).

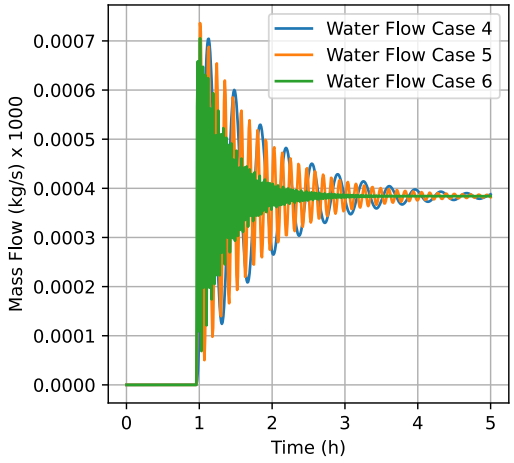

Figure 8. Parametric results water flow rate (cases 4 to 6).

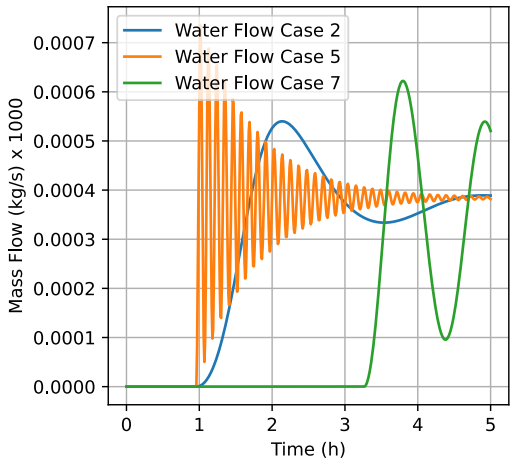

Figure 9. Parametric results water flow rate (cases 5 and 7).

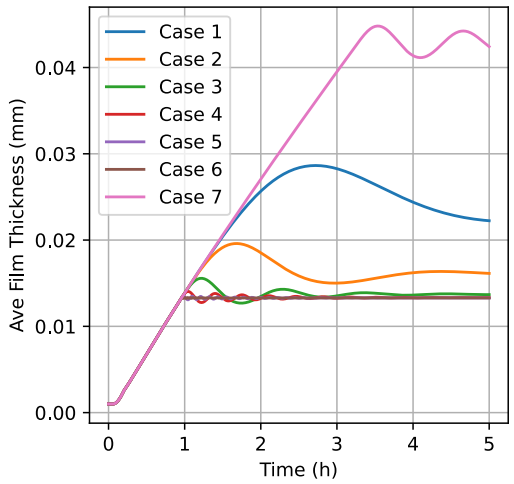

Figure 10. Parametric results average film thickness.

ature boundary condition. It also exercises all the connections of the surface model. The convective heat transfer coefficient being applied on the external side (right side, see figure 11) of the plate is so large that it acts as an infinite sink, nearly reaching the boundary condition temperature. The temperature profile represents a flight from a cold to a hot location. It reflects a winter to summer flight (across the equator). The mass of water on the surface is initially liquid, freezes in flight, and thaws as the flight arrives at the hot location. To further validate the

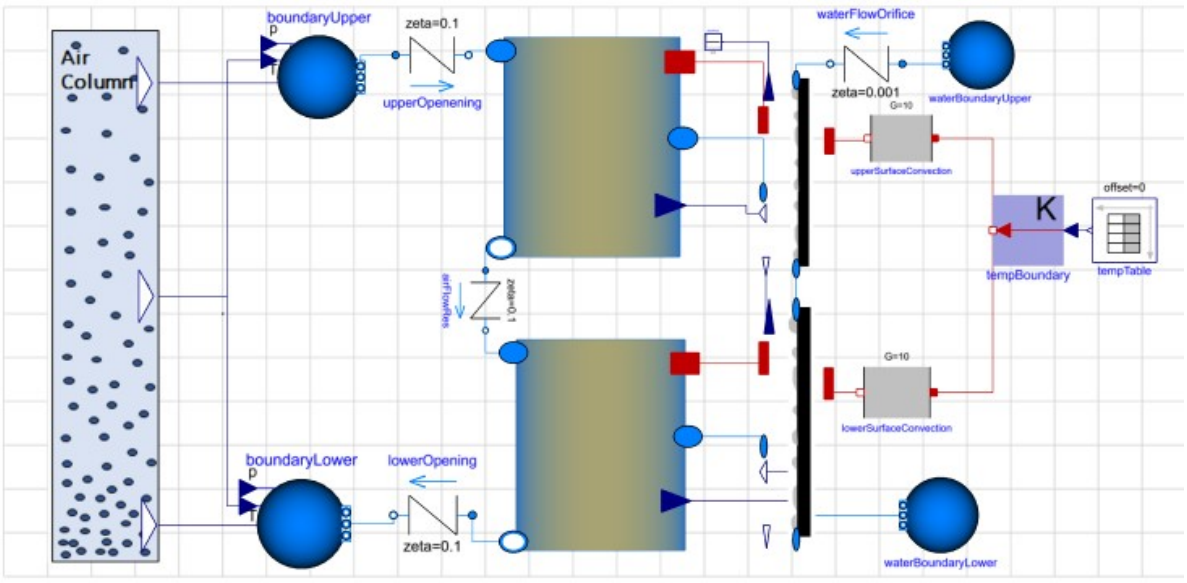

Figure 11. The complete model.

component behavior, this model includes an upper gap, a lower gap, an upper surface, and a lower surface (see figures 11 and 13). The model calculates the upper and lower opening pressure boundary with a buoyant air column of uniform temperature. The upper and lower openings are modeled using a simple generic orifice from the Modelica Fluid library. The fixed boundary fluid source named "waterBoundaryUpper" is only included to close the water flow network, its flow rate is zero.

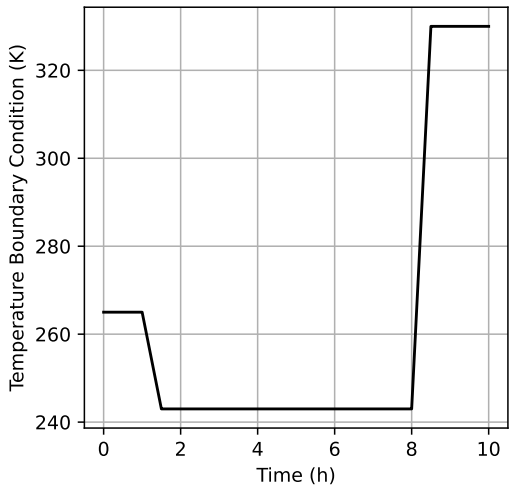

Figure 12. Realistic Temperature Profile.

The model simulates two connected sections of skin and insulation, with moist air and water flowing from the upper skin and air gap to the lower skin and air gap (see figure 13). Figures 14 to 20 show the thermodynamic state of the water, the droplet growth, and the flow rate of the water on the surface. The following observations can be made from figures 15 to 21: 1) the largest droplet diameter will increase when the surface temperature is below the freezing point of water beyond the critical droplet diameter, 2) upon melting gravity will quickly drain the water, 3) eventually evaporation will dominate the mass transfer, and 4) by the end of the flight the largest droplet diameter will be significantly diminished.

Elaborating on observation 1, the critical droplet diameter is reached when the gravity acting on mass of water in droplet is greater than the adhesion force securing the droplet to the surface. However, the model applies a scaling factor to the adhesion force to prevent water from draining when the surface temperature is below the freezing point of water. This allows the largest diameter of the surface to exceed the critical droplet diameter. See figures 15 and 19.

Regarding observation 2, the water drains until the critical diameter is reached. Figure 16 indicates that this occurs when the diameter is 0.82 mm. Figure 20 reveals that this happens 8.25 hours and 8.3 hours into the flight for the upper surface and lower surfaces, respectively.

According to observation 3, evaporation is the primary means of water removal once the critical diameter has been reached. Figure 17 shows that most of the mass flow of the water occurs as evaporation. A comparison of figures 20 and 21 reveals that while the peak mass flow rate of the drainage phase is larger than the evaporation rate, the integral of the evaporation is still larger than the integral of the drainage flow.

Finally, observation 4 exposes the limitations of the Modelica implementation method used for this model. The model required a minimum water mass control parameter to prevent solver instability as the surface dried. The sudden inflection at 9.2 hours (see figures 16 and 21) occurs because the actual mass of water on the surface is nearing the minimum mass.

The results verify that the buoyant air volume and the

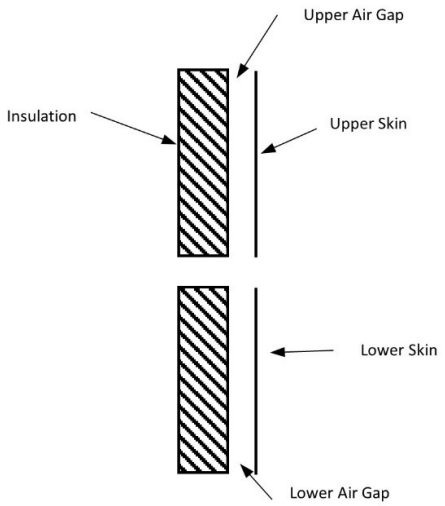

Figure 13. The complete simulation insulation system.

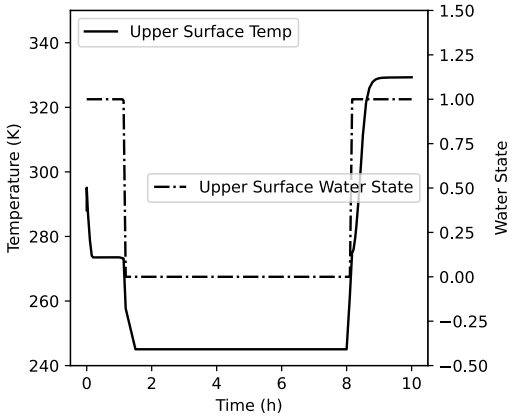

Figure 14. The temperature of the upper surface and the state of its water droplets.

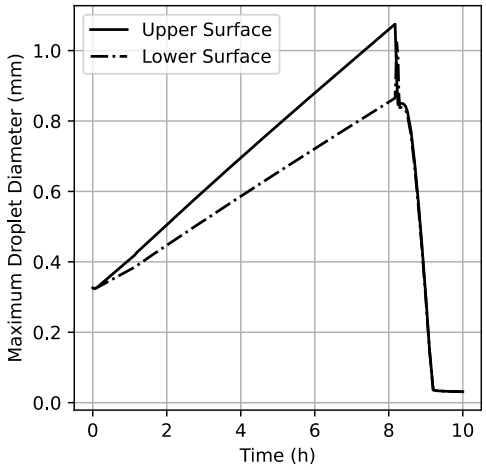

Figure 15. Size of the largest droplet on each surface throughout the flight.

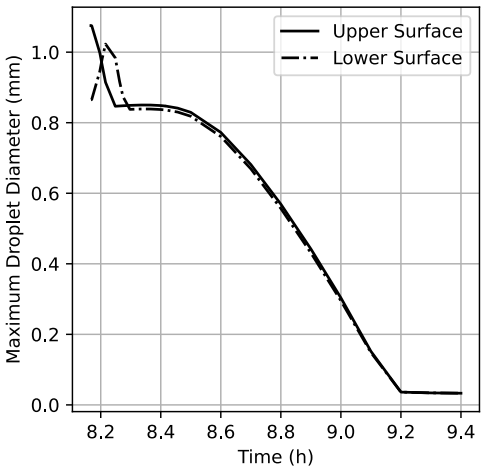

Figure 16. Size of the largest droplet after water has melted.

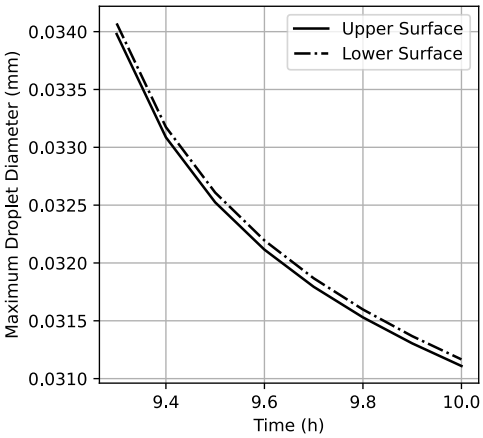

Figure 17. Size of the largest droplet at the end of the flight.

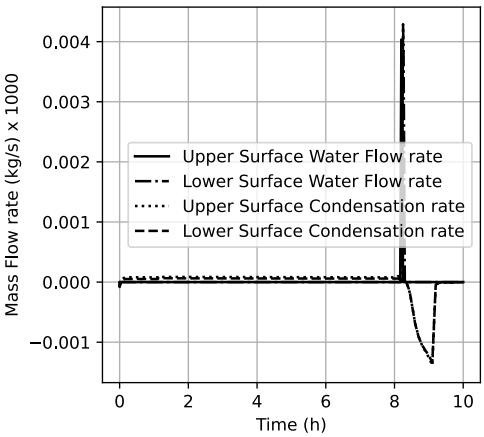

Figure 18. Drainage and condensation rates on each surface throughout the flight.

surface models can be combined to represent a system of connected channels and surfaces. The model runs quickly enough to accommodate any industrially meaningful time scale. Though an actual industrial scale analysis of an aircraft will include orders of magnitude more channels and surfaces. Condensation occurs very slowly in this exam-

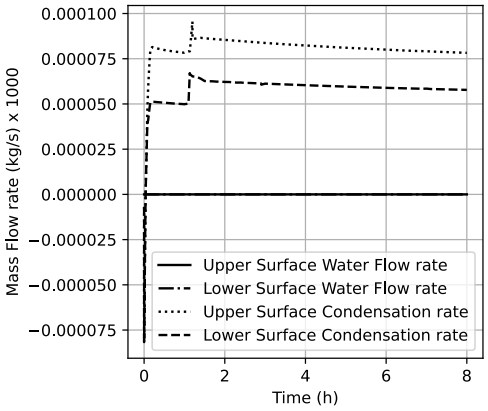

Figure 19. Condensation rates while the surface is frozen.

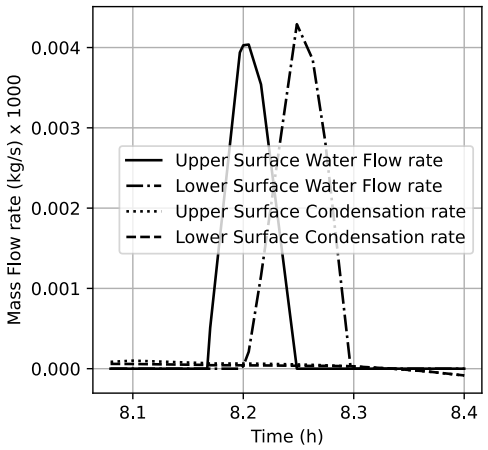

Figure 20. A zoomed in view of the drainage phase.

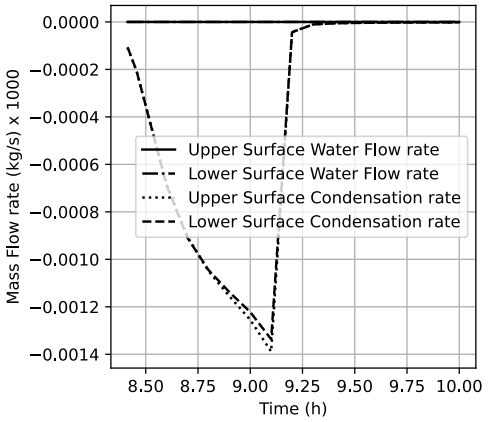

Figure 21. A zoomed in view of the evaporation phase.

ple. This agrees with industry experience, that undesirable conditions must persist over days to present an operational problem. The upper and lower surface temperatures were dropped below the freezing pointss of water in flight and are raised upon landing to exercise the evaporation functionality of the model. In summary, figure 14 shows that when the model transitions from frozen to liquid water without stability issues. Figure 15 demonstrates that the model simulates all the stages of the condensation process as expected. Figures 18 to 21 show how drainage and evaporation relate, that drainage occurs as a short term event while evaporation or condensation is always occurring.

Having simulated the droplet motion, the model may now be used to determine how much time is needed to evaporate the remaining water on the surface. This allows a more accurate prediction of the moisture load to which the insulation is exposed. Furthermore, a diffusion model could be applied to estimate the diffusion across the insulation lining.

The model was run using the desktop version of Modelon Impact (R). The solver selected was the CVode solver. It was run on PC with 2 Intel® Core^{TM} i7-557U CPUs @ 3.1GHz. The model took 3.3 minutes to run.

5 Conclusion

The reduced-order model described in this paper provides a means of estimating the residual moisture on a surface, has a very low computational requirement, and runs in minutes. Furthermore, it has been verified by comparison with a CFD model. It offers an advantage over CFD methods in that it can be easily applied to aircraft skin and insulation moisture modeling with large time scales. The 1-D model can be used to predict the residual water content at the end of a flight using the factors ζ, η, v_f. This model will support integration with a modeling ecosystem for product design, verification analysis, and digital twin methods. It supports moisture management system modeling for the day-to-day operation of an aircraft; i.e., the cycle of wetting, freezing, frost growth, thawing, draining, and drying. A standard water model that is valid below the freezing point would have simplified this drainage model.

Acknowledgements

The authors would like to thank Pieter Dermont of Modelon for his support with implementation of the software.

References

Arthur, Richard et al. (2020). *Digital twin: definition value*. Tech. rep. AIAA, pp. 1–16. URL: https://www.aia-aerospace.org/report/digital-twin-paper/.

Casella, Francesco et al. (2006). "The modelica fluid and media library for modeling of incompressible and compressible thermo-fluid pipe networks". In: *Proceedings of the 5th International Modelica Conference*, pp. 631–640. URL: https://elib.dlr.de/47217/.

Connell, William J, Cameron L Carnegie, and Marcus K Richardson (2020). *Air drying system and method therefor*.

Connell, William J and Marcus K Richardson (2022). *Test cage for testing a gap in a vehicle*.

Graham, Clark and Peter Griffith (1973). "Drop size distributions and heat transfer in dropwise condensation". In: *International Journal of Heat and Mass Transfer* 16.2, pp. 337–346. ISSN: 00179310. DOI: 10.1016/0017-9310(73)90062-8.

Grooten, M. H.M. and C. W.M. Van Der Geld (2012-04). “Surface property effects on dropwise condensation heat transfer from flowing air-steam mixtures to promote drainage”. In: *International Journal of Thermal Sciences* 54, pp. 220–229. ISSN: 12900729. DOI: 10.1016/j.ijthermalsci.2011.12.004.

Gu, L. D., J. C. Min, and Y. C. Tang (2018). “Effects of mass transfer on heat and mass transfer characteristics between water surface and airstream”. In: *International Journal of Heat and Mass Transfer* 122, pp. 1093–1102. ISSN: 00179310. DOI: 10.1016/j.ijheatmasstransfer.2018.02.061.

Huber, Paul, Karl Schuster, and Rob Townsend (1999). “Nuisance moisture”. In: *AERO*. URL: https://www.boeing.com/commercial/aeromagazine/aero_05/m/m01/index.html.

Khashayer, Borumand et al. (2019). *Modular environmental control chamber*.

Lents, Charles (2021). “Impact of weight, drag and power demand on aircraft energy consumption”. In: *AIAA Propulsion and Energy Forum, 2021*, pp. 1–6. DOI: 10.2514/6.2021-3322.

Liu, Jing, Hiroyoshi Aizawa, and Hiroshi Yoshino (2004). “CFD prediction of surface condensation on walls and its experimental validation”. In: *Building and Environment* 39.8, pp. 905–911. DOI: 10.1016/j.buildenv.2004.01.015.

Meyer, H et al. (2020). “Development of a digital twin for aviation research”. In: *Deutscher Luft- und Raumfahrt Kongress*, pp. 1–8. URL: https://elib.dlr.de/136848/.

Norrefeldt, Victor, Gunnar Grün, and Klaus Sedlbauer (2012). “VEPZO - velocity propagating zonal model for the estimation of the airflow pattern and temperature distribution in a confined space”. In: *Building and Environment* 48.1, pp. 183–194. ISSN: 03601323. DOI: 10.1016/j.buildenv.2011.09.007. URL: http://dx.doi.org/10.1016/j.buildenv.2011.09.007.

Pilat, D. W. et al. (2012-12). “Dynamic measurement of the force required to move a liquid drop on a solid surface”. In: *Langmuir* 28.49, pp. 16812–16820. ISSN: 07437463. DOI: 10.1021/la3041067.

Richardson, Marcus K, Brian T Imada, and Eric L Sarinas (2021). *Passive moisture management bladder in an aircraft*.

Rose, J. W. (1976). “Further aspects of dropwise condensation theory”. In: *International Journal of Heat and Mass Transfer* 19.12, pp. 1363–1370. ISSN: 00179310. DOI: 10.1016/0017-9310(76)90064-8.

Rose, J. W. and L. R. Glicksman (1973). “Dropwise condensation-The distribution of drop sizes”. In: *International Journal of Heat and Mass Transfer* 16.2, pp. 411–425. ISSN: 00179310. DOI: 10.1016/0017-9310(73)90068-9.

Seshia, Sanjit A. et al. (2017-09). “Design automation of cyber-physical systems: challenges, advances, and opportunities”. In: *IEEE Transactions on Computer-Aided Design of Integrated Circuits and Systems* 36.9, pp. 1421–1434. ISSN: 02780070. DOI: 10.1109/TCAD.2016.2633961.

Al-Sharafi, Abdullah et al. (2020-01). “Adhesion of a water droplet on inclined hydrophilic surface and internal fluidity”. In: *International Journal of Adhesion and Adhesives* 96, pp. 1–10. ISSN: 01437496. DOI: 10.1016/j.ijadhadh.2019.102464.

Steeman, H. J. et al. (2009). “Evaluation of the different definitions of the convective mass transfer coefficient for water evaporation into air”. In: *International Journal of Heat and Mass Transfer* 52.15-16, pp. 3757–3766. ISSN: 00179310. DOI: 10.1016/j.ijheatmasstransfer.2009.01.047. URL: http://dx.doi.org/10.1016/j.ijheatmasstransfer.2009.01.047.

Sun, Yujin et al. (2020-04). “Spreading and adhesion forces for water droplets on methylated glass surfaces”. In: *Colloids and Surfaces A: Physicochemical and Engineering Aspects* 591, pp. 1–9. ISSN: 18734359. DOI: 10.1016/j.colsurfa.2020.124562.

Sztipanovits, Janos et al. (2012). “Toward a science of cyber-physical system integration”. In: *Proceedings of the IEEE*. Vol. 100. 1. Institute of Electrical and Electronics Engineers Inc., pp. 29–44. DOI: 10.1109/JPROC.2011.2161529.

Weisensee, Patricia B. et al. (2017). “Condensate droplet size distribution on lubricant-infused surfaces”. In: *International Journal of Heat and Mass Transfer* 109, pp. 187–199. ISSN: 00179310. DOI: 10.1016/j.ijheatmasstransfer.2017.01.119.

Wörner, Mario et al. (2002). “Theoretical and experimental investigation of the humidity transport in aircraft cabins”. In: *8th AIAA/ASME Joint Thermophysics and Heat Transfer Conference*, pp. 1–11. ISBN: 9781624101182. DOI: 10.2514/6.2002-3023.